HEFAT2007
5th International Conference on Heat Transfer, Fluid Mechanics and Thermodynamics
Sun City, South Africa
Paper number: BS2

THE USE OF WEAK WAVES AS DIAGNOSTIC TRACERS IN UNSTEADY FLOWS

Beric W Skews [1] and Harald Kleine[2]
[1]Flow Research Unit, School of Mechanical, Industrial, and Aeronautical Engineering,
University of the Witwatersrand, Johannesburg, 2050, South Africa, beric.skews@wits.ac.za
[2]School of Aerospace, Civil, and Mechanical Engineering,
University of New South Wales, Australian Defence Force Academy, Canberra, ACT 2600, Australia

ABSTRACT

This paper examines the tracing of the trajectories of weak waves behind a shock wave induced flow in order to establish how the domain shape influences the flow both from a spatial and temporal perspective. The basic principle is that if a particle produces a series of point disturbances in a flow field the perturbations induced will propagate outwards at the local sonic velocity whilst at the same time being convected along with the local flow velocity. A number of issues may be identified for an unsteady flow. Firstly the flow field at later times may be influenced by perturbations produced at earlier times. Secondly, if the positions of the perturbations can be monitored as a function of time then the trajectory and velocity of the particle may be deduced. Thirdly, if a perturbation arises from a point on a boundary then its influence, if any, on any particular part of the flow can be established.

INTRODUCTION

The technique of placing small perturbations on the wall of a supersonic wind tunnel to evaluate the flow uniformity and to determine the Mach number from the measurement of the Mach angle in a steady flow is well known. An extension of this is shown in the steady flow of Fig. 1, where very shallow triangular grooves are placed on the body in order to establish local surface Mach numbers from the Mach angles, and particularly to give an indication of where the flow around the nose reaches sonic velocity, i.e. where the Mach lines become perpendicular to the body surface.

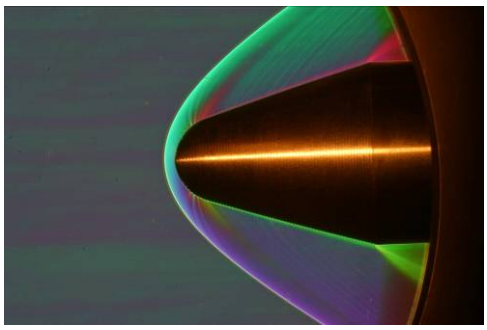

Figure 1. Colour schlieren image showing Mach lines emerging from the surface of a body. M= 2.4.

The same idea may be extended to unsteady flows. The nature of the perturbed flow field induced by a particle moving in a straight line in a compressible medium is a standard textbook illustration of the distinction between subsonic, sonic, and supersonic flow as shown in Fig. 2. Consider a particle which emits a pulse at regular intervals starting at a given point in time and in a uniform flow field. Each pulse will propagate outwards at sonic velocity in all directions with the centre of its circle of influence at the position where the pulse was emitted. As the point moves so a series of waves is produced. For a field which is stationary with respect to the particle a series of concentric waves will be produced. For a subsonic flow the presence of the particle is communicated to the whole field, with the waves being compressed in the direction of motion and expanded in the other direction giving rise to the Doppler effect. At particle sonic velocity, however, the field ahead of the particle has no knowledge of the particle or its motion until the piled up compression passes by. For supersonic flow this region of silence is even more extensive and an observer behind the particle will only become aware of its presence after the wave envelope has passed. It is on the basis of this sketch that the Mach number distribution and sonic point position may be estimated from images such as that in Fig. 1.

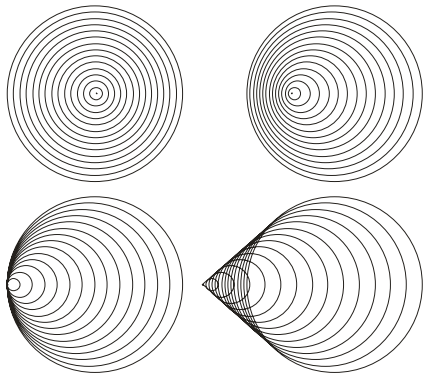

Figure 2 Perturbation fields for a particle at rest, subsonic velocity, sonic velocity, and supersonic velocity.

Lilley [1] has expanded on these patterns by considering acceleration and deceleration of a particle moving in a straight

line. This may be generalised even further by considering a particle moving in a curved path in unsteady motion. Consider a particle starting from rest, moving along a two-dimensional curved path, and accelerating through sonic velocity whilst sending out discrete perturbations at fixed intervals as shown in Fig. 3. This illustrates a number of issues. Firstly the flow field at later times is influenced by perturbations produced at earlier times even if the particle is moving at supersonic velocity. Secondly, if the positions of the perturbations can be monitored as a function of time then the trajectory and velocity of the particle may be deduced. Thirdly, if a perturbation arises from a point on a boundary then its influence, if any, on any particular part of the flow can be established.

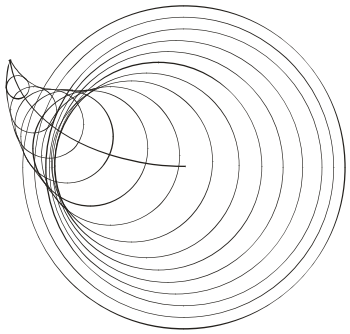

Figure 3 Perturbation field for a particle starting from rest and accelerating to supersonic velocity.

SHOCK WAVE INDUCED PERTURBATIONS

When a plane shock wave moves down a constant area duct and passes over a small two-dimensional wall imperfection a perturbation will be introduced in the following flow as indicated in Fig. 4 at a time *t* after the shock has passed over the imperfection. The flow behind the shock is uniform in velocity and sound speed and thus the propagating disturbance will remain circular with a radius *at*, where *a* is the post-shock sound speed. In the same time the shock will have moved a distance *Vt*, and the perturbation centre a distance *ut* from the source, where *V* and *u* are the shock and gas velocity respectively. Applying the standard plane shock wave equations in a frame of reference fixed in the tube wall both the velocity and sound speed behind the shock may be calculated. Thus the radius of the perturbation and its centre can be established as shown. The position where the perturbation strikes the shock, i.e. defining that part of the shock which is aware of the wall perturbation, is quantified by the angle *m*. An analytical equation for *m* as a function of shock wave Mach number M_s has been derived [2] and is given by:

$$\tan^2 m = (\gamma-1)\left(M_s^{\,2}-1\right)\left\{M_s^{\,2}+2/(\gamma-1)\right\}/(\gamma+1)M_s^{\,4}$$

where γ is the specific heat ratio. The angle α between the perturbation signal where it meets the shock and the incident shock may also simply be established from the geometry.

$$\cos\alpha = M_s a_0 / a - M$$

where a_0 is the sound speed ahead of the shock and *M* is the flow Mach number induced behind the moving shock.

It is noted that the angle *m* is very sensitive to Mach number for weak waves. An example of such a flow is given in Figure 5. Here a shock wave is diffracting around a 165° convex corner. An associated expansion wave propagates back up the duct into the oncoming flow, indicating that it is subsonic as well as reflecting off the top wall of the shock tube. The head of this wave corresponds exactly to the perturbation wave shown in Fig. 4 with the corner acting as the source of the perturbation. A number of small strips of thin tape are positioned transversely on the wall just before the corner resulting in a series of weak waves being shed from their edges and propagating into the flow. Their distortion gives some indication of the diffraction flow. However, they weaken as they expand outwards and soon become indistinguishable. An additional strip of tape is placed downstream of the corner, and the weak perturbation is evident. Its geometry in association with Fig. 4 may be used to determine the Mach number of the diffracted wave at the wall. It should also be noted that if the post-shock flow were supersonic the upstream wavelets would not be able to propagate into the oncoming flow and would be swept downstream as shown for the supersonic case in Fig. 2, with a Prandtl-Meyer expansion wave developing at the corner accelerating the flow still further. This occurs when the incident shock wave Mach number is greater than 2.068.

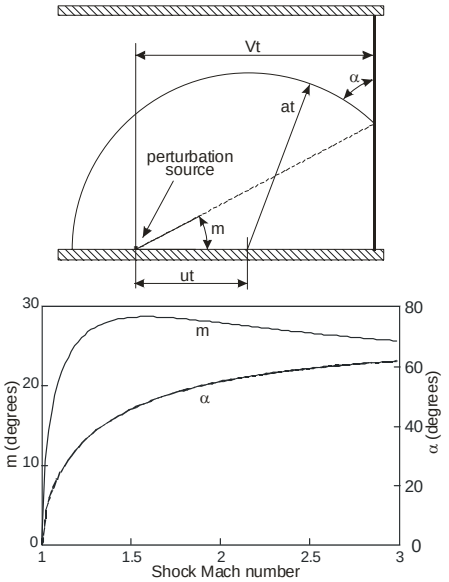

Figure 4 Acoustic perturbation resulting from a shock wave passing over a wall imperfection.

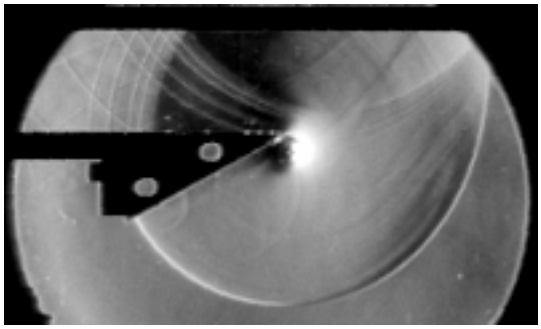

Figure 5 Schlieren photograph of a shock wave diffracting around a convex corner. M_s=1.28

GRID PERTURBATIONS

Consider the impact of a shock wave on a porous grid made up of a series of transverse bars. Three examples are given in Fig. 6. The left shadowgraph is for oblique impact on a 20% blockage grid, with an incident shock Mach numbers of 1.36. Blockage is defined as the ratio of the overall area closed to flow and the total area. Thus 100% blockage is an impermeable surface, and 0% represents no restriction to the flow. The rightmost pair of images are interferograms with a 67% grid blockage. The first of them shows Mach reflection and the second a regular reflection. In both cases the black fringes, which are lines of constant density, take on a zig-zag pattern as they pass through the perturbed region, thereby giving an indication of the weakness of the perturbed waves arising from the surface.

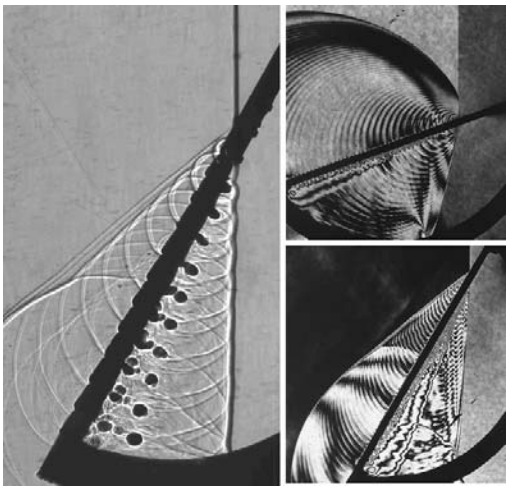

Figure 6 Images of shock wave interaction with a grid. Left: Shadowgraph [3]. Right: Interferometry [Courtesy: K Takayama, Tohoku University]

In order to assist in the analysis it is necessary to illustrate some of the basic flow features. These are shown schematically in Fig. 7 where the pattern is similar to that of shock refraction through a gaseous interface.

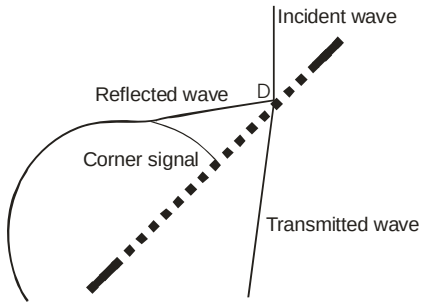

Figure 7 Main features of the grid interaction.

If, in a frame of reference fixed in the reflection point D, the flow between the reflected wave and the grid is supersonic, then this flow will have no knowledge of perturbations arising earlier in the motion, particularly those arising when the shock strikes the entry to the model. These disturbances propagate up the surface behind what is known as the corner signal. Where this corner signal reaches the reflected wave it separates the plane reflected wave from the curved portion which reflects off the solid entry section of the model. Corner signals are clearly visible in Fig. 6, except for the Mach reflection case. In that case the flow behind the reflection point is subsonic relative to point D, the reflected wave is curved, and perturbations arising throughout the disturbed flow influence the nature of the reflection. In the cases where the corner signal does not reach the reflection point the flow can be analysed in a frame of reference fixed in point D, using steady flow oblique shock analysis to determine the streamline pattern and thus the direction and magnitude of the inflow into the plate.

An alternative method is to examine the motion of the wavelets, which as indicated in the interferogram, are very weak. These waves are nearly circular and it is evident in examining the images that the centre of the circle is below the surface of the plate, thereby giving an indication of the direction of the inflow. On the other hand at the entry to the model where there are no slits the wavelet is perpendicular where it meets the surface. When the shock passes over a corner of any particular slit a wavelet is generated. Since the velocity of the shock wave is known the time taken for any particular wavelet to have reached the position in the photograph is known, and thus the velocity of the inflow may also be determined. An example of such an analysis [4] is reproduced in Fig. 8.

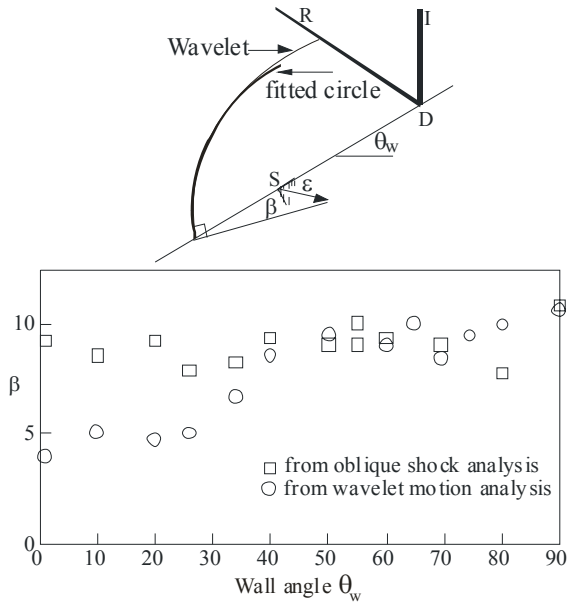

Figure 8 Inferred inflow angle

The agreement between the two methods is good for wall angles above 40 degrees but then deteriorates below this value. This is not surprising since at the lower wall angles the reflected shock is no longer plane and regular reflection analysis becomes inappropriate. For these cases the data from the wavelet measurement is thus more reliable. It is important to note that the shallow inflow angle is measured in a frame of reference fixed in the reflection point. For absolute entry angles

relative to the plate, angle ε in Fig. 8, the frame of reference has to be shifted.

An interesting feature is noted in the second shadowgraph image in that a second reflected wave is visible a short distance behind the first. This arises due to wavelet re-reflection from the bottom of the slits. Similar analyses can be done for the transmitted wave although care has to be taken in distinguishing between the waves generated at the upper and lower surface of each slit. However since the shed vortices under the plate move at particle velocity tracking them is more useful in determining the gas velocity.

FOAM AND POROUS BLOCKS

Consider the impact of a plane shock wave on a porous foam slab. Figure 9 shows a series of schlieren photographs taken 100 μs apart. These clearly show a myriad of wavelets propagating out from the pores as the flow enters the slab and is slowed down due to friction and multiple reflections from within the pore structure. In this case the pores are randomly distributed and the source for any particular wave cannot be established.

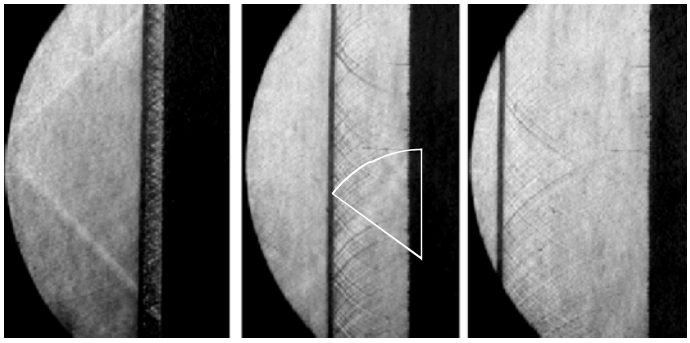

Figure 9 Various stages of reflected wave development following shock wave impact on an elastic porous foam block

However, some useful information may still be derived. Firstly it is noted that fitting a circular arc to the perturbations, its centre lies behind the foam face thereby giving a measure of the gas inflow. The spacing of the perturbations also gives an indication of the effective pore size. Secondly, an estimate may be made of the angle α between the shock front and the wavelet, as defined in Fig. 4. This is found to correlate reasonably well with measurements taken of arrival times measured by side-wall pressure transducers. Useful additional information could be obtained since the reflected wave accelerates as the successive compression waves within the foam coalesce to eventually form a constant strength reflected wave. Higher resolution images than the example given here would be needed for this technique to give accurate quantitative data.

A slightly stronger wavelet arriving from the top and bottom of the specimen and propagating towards the centre is noted. This is the corner signal generated at the moment of impact generated at the corner between the specimen and the upper and lower shock tube walls. Since its origin is known, as is the time at which the image is taken, information on sound speed and its variation could also be determined if high-speed time-resolved imaging were to be used. At later times, the situation becomes somewhat more complicated as the compressed foam plug starts moving down the tube.

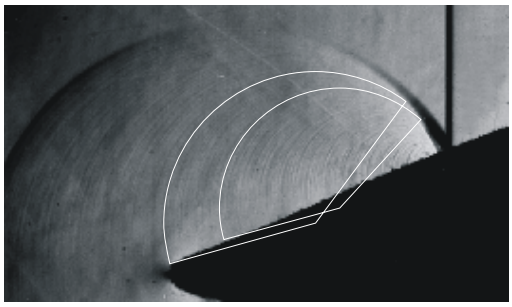

Figure 10 Shock wave impingement on a foam wedge.

Similar analyses can be done for shock impact on an inclined foam surface as shown in Fig. 10. Although the perturbations are very weak some estimate of the inflow may be made for wavelets generated at different times as the shock propagated over the surface. Of particular importance, however, is the distinct thickening of the reflected shock wave as the wavelets coalesce to form a compression wave. Unfortunately such tests become less useful at longer times due to the transverse collapse of the specimen arising from the foam dragging on the walls once it starts moving.

SHOCK REFLECTION FROM SURFACES

Very instructive results may be obtained from the study of the wavelets generated from the reflection of a shock wave from a curved surface. Figure 11 shows two images taken forty microseconds apart using a high framing rate digital camera. The first shows a Mach reflection off the shallower part of the surface and the second a transitioned regular reflection [5].

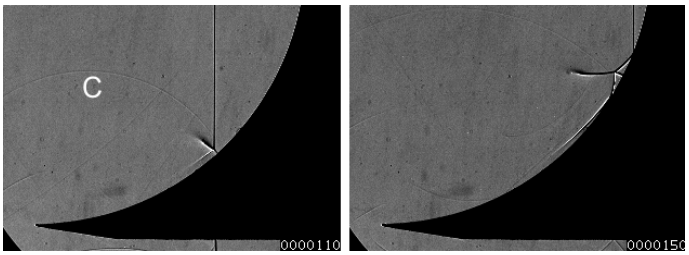

Figure 11 Shadowgraph images of shock wave reflection from a circular arc surface. Incident shock Mach number =1.24. C is the weak corner signal arising from the inlet.

Figure 12 shows later motion with the merging of the wave systems on the axis of symmetry. This has important implications relating to the mechanisms for focusing of non-linear waves, which has a number of practical applications such as in lithotripsy.

For the purpose of the current discussion two issues are of significance. Although the leading edge of the circular arc model is sharp it still causes a sufficient disturbance to generate a very weak corner signal (C) which is just discernable in the images of Fig. 11. This is important as it delineates the boundary between the flows that are influenced by the presence

of the surface from the uniform flow that is outside its region of influence and has been induced behind the incident wave. The second issue is that the reflected wave in all images appears to broaden out and then terminate in space so that the cause of its development is not apparent.

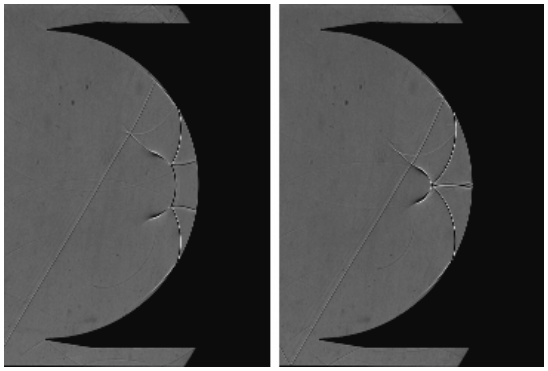

Figure 12 Focussing of the wave system on the axis of symmetry for a cylindrical cavity. Incident shock wave Mach number = 1.21

The question that arises is what the physical mechanisms are for this behaviour. Some indication of the reason can be found in Fig. 13, which is an example of a grid test such as shown in the top left image of Fig. 6, but which had inadvertently been photographed at a much later stage. In this photograph the incident shock propagated from the left of the frame. The focusing of the flow into a complex shock wave structure is evident, and consists of a pair of wall shocks and reflected waves arising from the transitioned regular reflection, as shown in Fig. 11, from either side of the cavity. Of major interest is the way in which the wavelets coalesce into the reflected wave thereby giving a strong indication that its formation is due to the compressive signals arising from various points on the domain boundaries, combining to form a shock wave. However, individual images such as this do not give any indication of the source or the propagation of the individual wavelets.

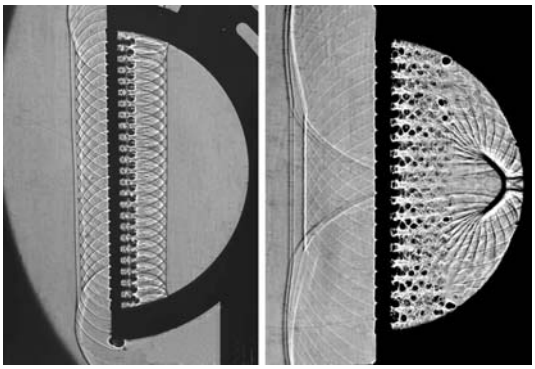

Figure 13 Development of shock propagation through a grid and impingement on a cylindrical surface.

An ideal manner in which to study the temporal growth of the various features, particularly relating to the important issue of wave focusing, is by time-resolved photography where the propagation of individual wavelets may be monitored as they propagate outwards from the wall. Highly sensitive shadowgraph and schlieren imaging techniques are required to resolve the wavelets which need to be arranged to be weak so that they travel close to the local sound speed.

In a current study on cylindrical and parabolic cavity profiles such perturbation sources are positioned by placing strips of 45 micron thick tape onto the wall. In the case of strong waves it is found that wall roughness can also act as a suitable source even though the surface has been smoothed to remove machining marks.

A Shimadzu HPV-1 high-speed digital camera was used to obtain the video clips. Framing rates were varied between 125 kfps and 1 Mfps (fps = frames per second) with exposure times per frame of between 250 ns and 1μs. 102 frames are obtained for each test. These clips can then be played back as video clips which then give an excellent understanding of the evolution of the flow. Single frames from some of these tests are given below.

Consider first the formation of the reflected wave as the incident shock enters the cavity as shown from a selection of frames for a single test given in Fig. 14. The numbers are the time, in microseconds, from when the shock strikes the leading edge. Since the slope of the cavity wall at entrance is parallel to the direction of incident shock motion the first perturbation will be exactly that analysed in Fig. 4, and, as noted before, is just visible in Fig. 11. In the test piece of Fig. 14 the leading edge has a small internal ramp which results in the initial signal consisting of a weak compression followed by a weak expansion. These are clearly evident in the first frame but soon merge into a single weak perturbation. As the wall turns towards the flow a whole series of individual compressive perturbations will be generated, with those generated at the small steps from the edges of the attached tape being visible. The interest is to see how these combine to generate the reflected wave.

It has generally been assumed in the past that all the compressive waves generated off the surface combine to form the reflected wave. This is clearly not the case. The first perturbation intersects the incident wave rather than merging with the subsequent wavelets. In the first frame the second and third wavelet start to combine causing the incident shock to bend forward near the wall with this curvature causing a strong gradient behind it. By the second frame the second to fourth waves have combined to form a reflected shock as is evident by the appearance of a slipstream indicating the existence of a three-shock configuration, i.e. a Mach reflection. This situation continues at the third frame with the interesting effect that some of the wavelets merge from one side of the reflected wave and others from the other side. At this time the incident wave has been completely reflected from the surface resulting in an imploding cylindrical wave. This collapses at the time shown in the fourth frame, which is referred to as the gas dynamic focus. The two wall shocks have also met at the axis of symmetry. They pass through each other, merge and form the main reflected wave from the cavity seen as the smoothly curved wave in the last two frames. It is noted that all the wavelets

generated earlier in the motion terminate on this wave, as is to be expected.

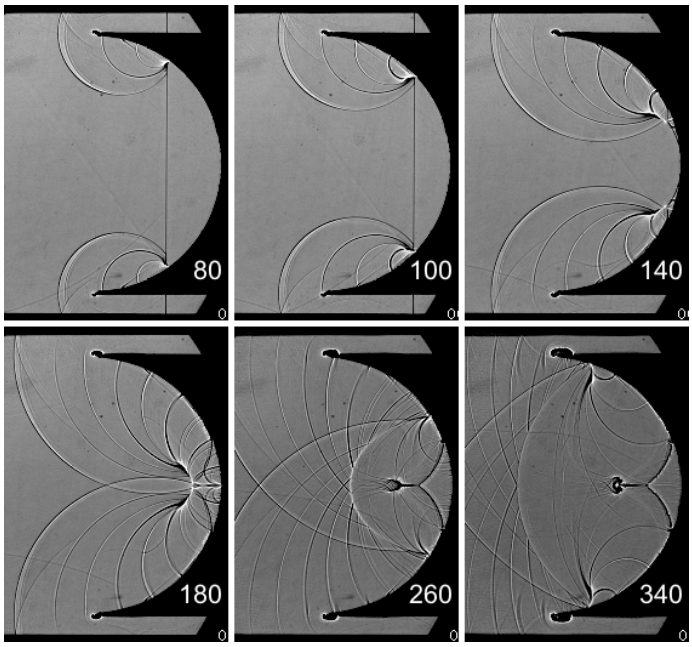

Figure 14 A Mach 1.33 shock wave impingement on a cylindrical cavity. Thin tape attached to the wall generates weak signals in the flow.

It is interesting to note that this reflected wave is not perpendicular to the wall and as it passes over the tape edges a new series of perturbations develop, which again coalesce into another reflected wave.

This method of experimentation graphically illustrates how signals propagate through the whole field. That the wavelets are very weak is confirmed by comparing images taken at the same Mach number for flows with and without the tape. It is confirmed that the presence of the tape does not influence the flow to any measurable extent.

Since schlieren imaging shows gradual density gradients which are missed in shadow photography it is useful to run tests using this technique as well. A typical example is given in Fig. 15, for a lower Mach number. An omni-directional optical system is used, with the background shading in the image giving an indication of the gradients.

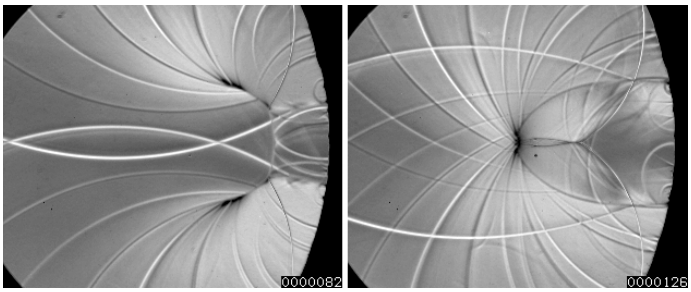

Figure 15 High magnification schlieren image for a Mach 1.22 incident shock reflection. Images taken 44 μs apart. The wave patterns should be compared to those in Fig. 12 in order to identify the main features.

What is interesting for this lower Mach number case is that the first perturbation propagates even further beyond the point where the three-shocks meet.

As a final example the case of reflection in a parabolic cavity is given in Fig. 16. The crossed waves at the left are the shocks arising at the lip of the cavity because there is no initial weak perturbation due to the finite wall angle at the entrance to the cavity. The reflection process is significantly different. The incident shock curves strongly forward increasing rapidly in strength. Significant perturbations are generated from the wall. In this case no tape is used and the waves are generated from surface roughness, even though the model had been finished with fine grade abrasive paper. Again the interesting phenomenon is noted how the wave curvature breaks into a discontinuity as the wavelets coalesce into a reflected shock, also resulting in a three-shock geometry with a very clear slipstream emanating from the intersection point.

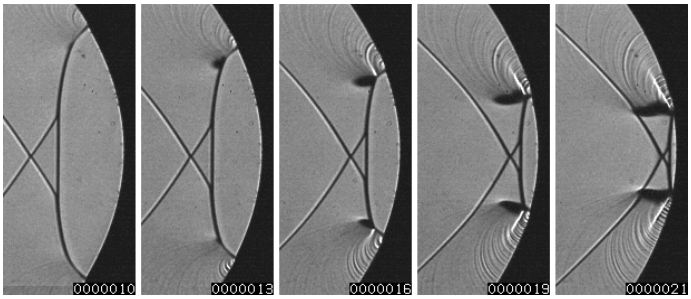

Figure 16 Wave pattern towards the base of a parabolic cavity. The wavelets arise from wall roughness. Images are taken 3 μs apart. Shock Mach number =1.23.

CONCLUSION

The technique of tracing weak signals in an unsteady flow has the promise of being a powerful diagnostic tool in understanding the mechanisms behind unsteady gas dynamic phenomena. It also has the potential to be used to construct reflection surfaces to generate a variety of pressure distributions and flow regimes. Simply rounding the entrance to a parabolic cavity has empirically been shown to have a major influence in this regard [6].

The technique will also be useful in conjunction with CFD where very weak waves are generally obscured in the numerical noise, and thus where regions of influence of the boundary geometry cannot be assessed.

REFERENCES

[1] Lilley G.M. and Yates A.H. Some aspects of noise from supersonic aircraft. *J. Roy. Aero. Soc*., 57, 396-414, 1953.

[2] Skews B.W. The shape of a diffracting shock wave. *J. Fluid Mech*. 29, 297-304, 1967.

[3]Skews B.W. Shock wave interaction with porous plates. *Experiments in Fluids*, 39, 5, 875-884, 2005

[4] Skews B.W. and Takayama K. Flow through a permeable surface due to shock wave impact. J. Fluid Mech. 314, 27-52, 1996

[5] Ben-Dor G. *Shock wave reflection phenomena*, Springer, 1992.

[6] Babinsky H., Onodera O., Takayama K., Saito T., Voinovich P. and Timofeev E. Influence of entrance geometry of circular reflectors on shock wave focusing. *Computers and Fluids*, 27, 611-618, 1998.